



## Development of a novel non-water infrared refractance window drying method for Malabar spinach: Optimization of process parameters using drying kinetics, mass transfer, and powder characterization

Durgawati, P. Balasubramanian & Parag Prakash Sutar

To cite this article: Durgawati, P. Balasubramanian & Parag Prakash Sutar (2023) Development of a novel non-water infrared refractance window drying method for Malabar spinach: Optimization of process parameters using drying kinetics, mass transfer, and powder characterization, *Drying Technology*, 41:10, 1620-1635, DOI: [10.1080/07373937.2023.2169865](https://doi.org/10.1080/07373937.2023.2169865)

To link to this article: <https://doi.org/10.1080/07373937.2023.2169865>



View supplementary material [↗](#)



Published online: 08 Feb 2023.



Submit your article to this journal [↗](#)



Article views: 314



View related articles [↗](#)



View Crossmark data [↗](#)



Citing articles: 1 View citing articles [↗](#)



# Development of a novel non-water infrared refractance window drying method for Malabar spinach: Optimization of process parameters using drying kinetics, mass transfer, and powder characterization

Durgawati<sup>a</sup>, P. Balasubramanian<sup>b</sup>, and Parag Prakash Sutar<sup>a</sup> 

<sup>a</sup>Department of Food Process Engineering, National Institute of Technology Rourkela, Odisha, India; <sup>b</sup>Department of Biotechnology and Medical Engineering, National Institute of Technology Rourkela, Odisha, India

## ABSTRACT

In the present work, a novel non-water Infrared Refractance Window drying (IR-RWD) method was developed for Malabar spinach. Experiments were conducted using a hybrid experimental design. Fresh Malabar spinach was pretreated using the vacuum steam pulsed blanching (VSPB) method. Results showed that VSPB inactivated POD and PPO activities to 9.77% and 5.42% within four cycles, respectively. The optimum conditions were found at 1.2 mm sample thickness, 40% infrared power, and 3.67 cm distance between IR emitter and glass plate resulting in 67.38 % chlorophyll retention, 7.72 overall color changes, 16.57 mgGAE g<sup>-1</sup> total phenolic content, and 11.20 kJ kg<sup>-1</sup> specific energy consumption. The Page model showed the best fit to the drying kinetics. Furthermore, Biot number indicated the impact of both internal and external resistance on moisture diffusivity. XRD and FESEM characterization of dried powder showed a semi-crystalline phase and square plate, porous morphology. The non-water IR-RWD was a promising alternative to traditional water RWD.

## ARTICLE HISTORY

Received 12 September 2022

Revised 29 November 2022

Accepted 9 January 2023

## KEYWORDS

Biot number; FESEM; FTIR; Microstructure; XRD


## 1. Introduction

All vegetables, including green leafy vegetables, are an important contributor to human nutritional needs and are a good source of phytochemicals, fibers, minerals, and vitamins.<sup>[1]</sup> Consumption of vegetables in the right amount helps to maintain proper health and prevents from many diseases.<sup>[2,3]</sup> Malabar spinach, a tropical leafy-green vegetable belonging to the *Basellaceae* family, is the richest source of essential amino acids, fiber, phenolic compounds, minerals, and vitamins.<sup>[4]</sup> Despite being nutritionally dense, it is still an underutilized and rarely consumed leafy vegetable. Due to its high perishability nature, it is challenging to keep it fresh for a prolonged time once harvested; therefore, most of it has to be discarded.<sup>[4]</sup> To obtain an economical source of a variety of crucial nutrients and reduce food loss, it is essential to examine the various strategies for preserving food. Drying an easy and efficacious preservation method, that inhibits the growth of microbial spoilage organisms and the deterioration reaction. The selection of a drying method for the plant-based material is important

to retain the nutritional and sensory properties of the product. Putriani et al.<sup>[5]</sup> reported that the hot air drying of green leafy vegetables, including spinach, resulted in the reduction of bioactive compounds like chlorophyll, ascorbic acid, and phenolic content. Researchers showed that the freeze-dried curry leaves powder retained higher chlorophyll content, but lower volatile components than the microwave-dried curry leaves powder.<sup>[6]</sup> A potential method for drying this sort of vegetable into a powder form is refractance window drying (RWD).

RWD is a fourth-generation drying system also known as a deviation window drying technology.<sup>[7]</sup> It is an efficient drying technology with a higher drying rate and uses radiative energy to dry the product. In RWD, the product, either in the form of pulp, puree, or paste, is spread over a Polyethylene Terephthalate (PET) sheet, which is placed above the hot water at a temperature between 90–95 °C, and a high-quality product is generated.<sup>[8]</sup> Santos et al.<sup>[9]</sup> reported that the RWD dried carrot possesses similar color, and total polyphenol content to the fresh carrot slices. The

**CONTACT** Parag Prakash Sutar  [sutarp@nitrkl.ac.in](mailto:sutarp@nitrkl.ac.in)  Department of Food Process Engineering, National Institute of Technology Rourkela, Odisha, India

 Supplemental data for this article can be accessed online at <https://doi.org/10.1080/07373937.2023.2169865>.

© 2023 Taylor & Francis Group, LLC

maximum retention (greater than 50%) of the bioactive compounds, including polyphenol content, antioxidant and anthocyanin were observed in RWD dried purple yam powder at 70 and 80 °C.<sup>[10]</sup> A window is formed between the PET sheet and the hot water touching the surface, allowing the infrared heat to flow through and dry the sample. Studies on RWD, tomato paste,<sup>[11]</sup> spinach, broccoli, and kale<sup>[12]</sup> have been notified. This research showed that the dried product obtained has high retention of nutrients and less drying time compared to the conventional drying method. Besides this, some disadvantages of the RWD process include the need for a hot water circulation system, maintaining the water temperature during the entire drying process, drainage issues, insulation devices, and expensive PET sheets. These factors also increase the energy consumption and overall cost of the operation. To overcome its limitation, a novel non-water-based Infrared Refractance Window Drying technology (IR-RWD) that uses tough glass plate instead of PET sheet can be a promising method. Application of infrared in drying will improve the drying efficiency of the process, reduce running costs, conserve energy during operation, and prevent water treatment and drainage issues.<sup>[13]</sup> In addition, replacing the PET sheet with an IR transmittable glass plate will reduce the cost and limit the use of plastic. Rajoriya et al.<sup>[14]</sup> stated that combining the RWD with far infrared resulted in shorter drying time, better quality retention, and energy efficiency.

In terms of quality comparison of RWD with other drying methods, it provides the customer with superior quality and high nutritional value products. The RWD dried cornelian cherry powders showed higher retention of ascorbic acid, total monomeric anthocyanin, color than the convective dried product.<sup>[15]</sup> The antioxidant activity and color of RWD dried golden-berry pulp was found similar to freeze dried product.<sup>[16]</sup> It also requires less drying time and improves drying efficiency.<sup>[17]</sup> RWD gave higher bulk density, rehydration ratio, solubility, and hygroscopicity values than convection drying of tomato powder.<sup>[18]</sup>

Drying of Malabar spinach has been explored using hot air drying, foam-mat drying, and microwave drying.<sup>[19,20]</sup> However, most of their work focused on investigating physical, chemical, and qualitative properties. An assessment of drying kinetics and mass transfer parameters is necessary for a successful drying operation.

Based on the literature survey, no work is being reported on replacing hot water with an electrical infrared lamp as a heating source and a PET sheet

with a glass plate in RWD. Also, Malabar spinach drying kinetics, moisture diffusivity, and mass transfer have not yet been investigated in the non-water IR-RWD method. Therefore, the objective of this research work was to develop a non-water IR-RWD method and optimize its process parameters with the insights using drying kinetics and mass transfer phenomenon and powder characterization by instrumental methods like XRD, FTIR, and FESEM.

## 2. Materials and methods

### 2.1. Raw material

Fresh Malabar spinach (species *Basella alba*) samples were obtained from a local market in Rourkela (Odisha, India). The leaf and stem were cleaned thoroughly under running water until the water stayed clear. The stem was chopped into smaller pieces. The initial moisture content of Malabar spinach was estimated by vacuum oven at 70 °C and was found to be 90% on a wet basis (wb).<sup>[21]</sup>

### 2.2. Pretreatment experiments

Before drying, Malabar spinach was treated using vacuum steam pulsed blanching (VSPB). Hot water blanching (HWB), and steam blanching (SB) are commercially adopted methods in the food industry. But due to some drawbacks like nutrient loss, poor efficiency, and wastewater generation, the uses of HWB and SB are limited. A new method, like VSPB, showing the positive effects on drying and quality of products, was opted for blanching in the present study.<sup>[22]</sup> Figure 1 shows the schematic diagram of VSPB experimental setup. The equipment consisted of a steam generator, vacuum pump, a blanching chamber with gasket and closure to prevent steam pressure leakage, and a control system. The vacuum was 20 kPa for 15 s followed by steam purging at 110 kPa for 20 s. This process was carried out until 5 blanching cycles were completed. The process conditions were fixed based on the preliminary trials for the inactivation of the polyphenol oxidase (PPO) and peroxidase (POD) enzymes. Also, these VSPB conditions were found to be supported by another study reported by Wang et al.<sup>[23]</sup>

The control HWB was performed by immersing Malabar spinach in 100 °C water for 120 s and control SB at continuous atmospheric pressure steam for 90 s.<sup>[24]</sup> PPO and POD were estimated after the pretreatments by using the method described by Kar and Sutar.<sup>[25]</sup> After blanching, the leaves and stem (3:1

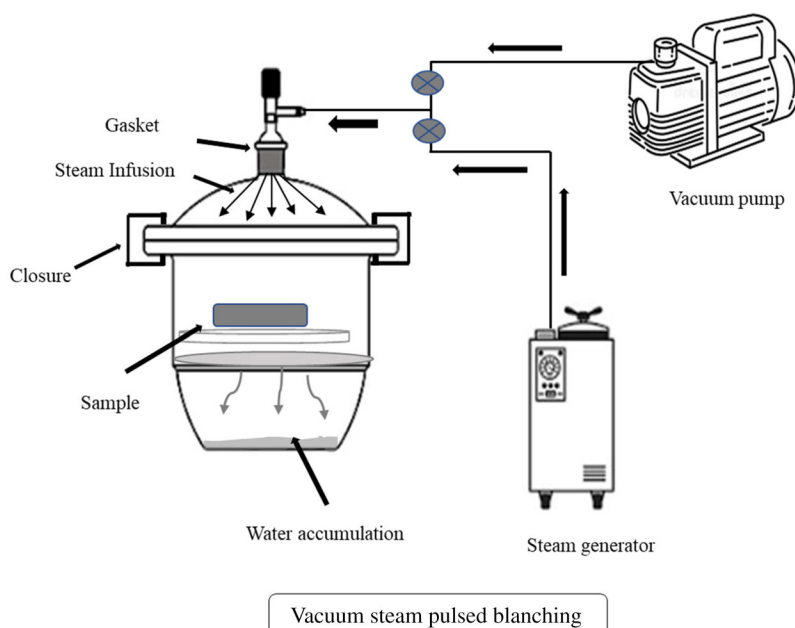


**Figure 1.** Vacuum steam pulsed blanching setup for fresh Malabar spinach.

ratio w/w) were taken and processed using a blender for 1 min until a homogeneous paste was obtained for further drying experiments.

### 2.3. Novel non-water infrared refractance window drying

During preliminary trials, it was observed that the total process time starting with water heating to drying of Malabar spinach paste in traditional RWD was significantly high. Approximately 1 h was required for achieving the 90–95 °C water temperature and 35 min for drying of 1 mm thick sample. In addition, the water recirculation and temperature maintenance during the entire process were additional tasks. Therefore, to eliminate the drawbacks associated with traditional RWD, the novel non-water IR-RWD was developed. The schematic diagram of the non-water IR-RWD experimental setup is shown in Figure 2. It consisted a stainless steel cabinet fitted with an electrical infrared emitter, an IR transmittable glass plate of 0.2 cm thickness, a stand for adjusting the distance between the emitter and the glass plate, and an exhaust fan. The IR emitter giving near-infrared (NIR) peak wavelength ranging from 0.78 – 1.4  $\mu\text{m}$  were used in the experiments due to its higher penetration depth.<sup>[26]</sup> The quartz tungsten IR emitter of 500 W (Litel Infrared Private Limited, Pune, India) was placed at the bottom of the drying chamber. The power of the electrical infrared emitter was mentioned in terms of the percentage of the full power of the emitter in Watts. Based on the preliminary trials

maximum of 100% power (500 Watt) and a minimum of 20% power (100 Watt) the IR emitter power were selected for the experiments.

The infrared power was controlled by a controller. An adjustable stainless-steel platform was used for maintaining the distance between the electrical infrared emitter and glass plate. The experiments were performed by placing the infrared emitter at the bottom and the known thickness of Malabar spinach paste sample on the glass plate positioned above the IR emitter at a known distance. The Infrared thermometer (KUSAM-MECO IRL380, Mumbai, India) was used for measuring the product temperature at multiple points of the sample and the average value was calculated and noted as the product temperature.

The experiments were planned using a hybrid design with three independent variables generating 15 treatments, including 5 center points. The independent variables were sample thickness ( $ST$ ), IR power ( $P$ ) and distance between the emitter and sample ( $D$ ). The range of the variables is given in Table 1. The responses collected were chlorophyll retention ( $CR$ ), overall color change ( $\Delta E$ ), total phenolic content ( $TPC$ ) and specific energy consumption ( $SEC$ ). The range of experimental parameters was based on results from preliminary trials. The optimization was done using response surface methodology in Design-Expert software (Stat-Ease, DX11). The optimized dried Malabar spinach powder was compared with the traditional RWD powder. A RWD lab-scale setup was developed using a hot water bath, PET sheet (0.175 mm thick) and an exhaust fan for drying

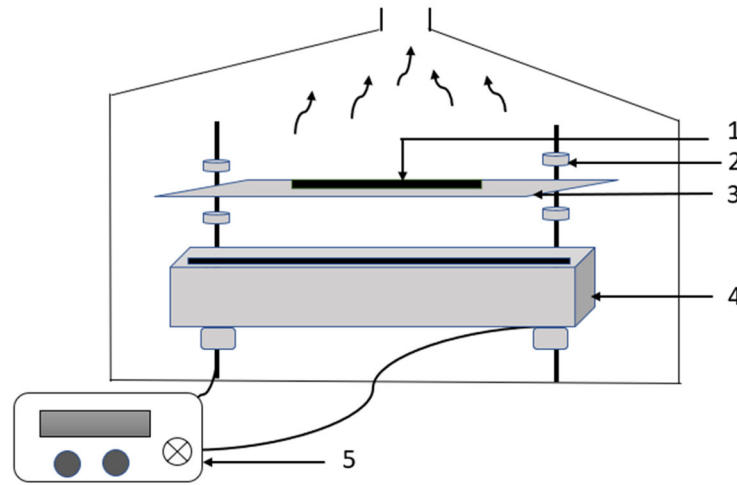


**Figure 2.** Schematic diagram of the experimental setup of non-water IR-RWD. (1) Malabar spinach paste sample; (2) height adjustable stand; (3) IR transmittable glass plate; (4) infrared lamp; and (5) IR Power controller.

**Table 1.** Coded and actual values of independent variables for non-water IR-RWD.

Independent parameter	Level				
	$-\alpha$	$-1$	$0$	$+1$	$+\alpha$
Sample thickness, mm (A)	0.6	1	2	3	3.42
Infrared Power, % (B)	21.71	30	50	70	78.28
Distance between IR emitter and glass plate, cm (C)	2.4	3.42	4.5	5.58	6.6

blanched Malabar spinach paste for comparison purpose. A thin layer PET film was placed over hot water bath. The lower side of the film was in touch with hot water; whereas the sample was spread on other side of the PET film in 1 mm thickness. The water bath temperature was set at 95 °C. The average product temperature was approximately 70 °C, and the sample was dried until weight change was negligible. After drying, the products were packed in airtight zip-lock polyethylene bags and stored at -4 °C for quality analysis.

#### 2.4. Modeling drying kinetics

The sample weight was recorded at the 2-minute intervals by using a precise weighing scale until the constant weight was achieved and the moisture content was estimated using mass difference. Fick's second law (Eq. (1)) was used to evaluate the moisture transport mechanism during drying considering the assumption (a) moisture is evenly distributed throughout the sample (b) mass transmission is proportional with regard to the center (c) diffusion is the mechanism that controls mass transfer

$$\frac{M_t - M_e}{M_t - M_0} = \frac{8}{\pi^2} \exp\left(-\frac{\pi^2 t D}{4x^2}\right) \quad (1)$$

where,  $M_t$ ,  $M_0$ , and  $M_e$  denotes moisture content of sample at time ( $t$ ), initial moisture content and equilibrium moisture content in dry basis,  $D$  is moisture diffusivity in  $\text{m}^2 \text{s}^{-1}$  and time ( $t$ ) in seconds and  $x$  is sample thickness.

Several mathematical models have been developed and used to describe the drying behavior of agricultural products but the Page model is most popularly used for studying the drying kinetics in infrared drying<sup>[13]</sup>

$$\text{MR} = \exp(-kt^n) \quad (2)$$

where,  $k$  is the rate constant ( $\text{min}^{-1}$ ),  $n$  is the model parameters, and  $t$  is the drying time (min). The evaluation of the model was done by estimating coefficient of determination ( $R^2$ ), and calculating root mean square error (RMSE).

#### 2.5. Estimating of mass transfer parameters

The mass transfer coefficient ( $h_m$ ,  $\text{m s}^{-1}$ ) was determined using the analytical approach proposed by Ibrahim Dincer & Dost et al.<sup>[27]</sup> Few assumptions were considered before applying the model. The sample and drying medium were supposed to have constant thermophysical properties. The influence of heat transfer on mass transfer was assumed minimal, and the moisture diffusivity occurs along the thickness of the sample as the Malabar spinach was spread in a layer (similar to the thin infinite slab). The one-dimensional apparent moisture diffusivity ( $D_a$ ) equation for an infinite slab can be written as follows

$$\frac{\partial}{\partial x} \left( \frac{\delta \text{MR}_{x,t}}{\delta X} \right) = \frac{1}{D_a} \frac{\partial \text{MR}_{x,t}}{\partial t} \quad (3)$$



The initial and boundary conditions are

$$MR(x, 0) = 1, \text{ for } 0.1 < B_i < 100 \text{ and } B_i > 100 \quad (4)$$

$$\frac{\partial}{\partial x} MR(0, t) = 0, \text{ for } 0.1 < B_i < 100 \text{ and } B_i > 100 \quad (5)$$

$$D_a \left[ \frac{\partial}{\partial x} MR(x, t) \right] = h_m MR(x, t), \text{ for } 0.1 < B_i < 100; MR(x, t) = 0, \text{ for } B_i > 100 \quad (6)$$

where,  $MR$  is moisture ratio and  $B_i$  is Biot number

The solution for Eq. (6), considering the initial and boundary condition yield dimensionless center moisture distributions in the form of Eq. (7) as,

$$MR = \sum_{n=1}^{\infty} A_n B_n, \text{ for } 0.1 < B_i < 100 \text{ and } B_i > 100 \quad (7)$$

Where,  $A_n$  and  $B_n$  depends on the sample geometry and are dimensionless number. For infinite slab, the  $A_n$  and  $B_n$  can be written as Eqs. (8)–(10)

$$A_n = \frac{2 \sin \mu_{Da}}{((\mu_n) + (\sin \mu_n \cos \mu_n))}, \text{ for } 0.1 < B_i < 100 \quad (8)$$

$$A_n = \frac{(2(-1)^{n+1})}{\mu_n}, \text{ for } B_i > 100 \quad (9)$$

$$B_n = \exp(-\mu_1^2 F_o), 0.1 < B_i < 100 \text{ and } B_i > 100 \quad (10)$$

The lag factor ( $J$ ) and drying coefficients ( $S$ ) were calculated by assuming that the dimensionless moisture distribution follows an exponential pattern

$$MR = J \exp(-St) \quad (11)$$

$$-\mu_1^2 F_o = St \quad (12)$$

Therefore, the following dimensionless number are introduced for the determination of diffusivity and  $h_m$ . Fourier number (Eq. (13)), used for the determination of diffusivity whereas,  $h_m$  was calculated from the Biot number that basically represents the ratio between the internal and external resistance (Eq. (14)).

$$F_o = \frac{D_a t}{x^2} \quad (13)$$

$$B_i = \frac{h_m x}{D_a} \quad (14)$$

$J$  and  $S$  values were determined by plotting Eq. (11) in Origin lab 2020a software and the best fit was identified by  $R^2$  and RMSE.

## 2.6. Quality evaluation of Malabar spinach powder

The chlorophyll content was estimated by the method given by Sadasivam & Manickam.<sup>[28]</sup> The sample (1 g) was pulverized using 80% acetone and was filtered using Whatman paper 1. The optical density (OD) was measured at 645 and 663 nm using a UV spectrophotometer (UV-1800, Shimadzu, Japan) and the chlorophyll retention was estimated in percentage. The color of dried MSP was assessed by using Hunter-Lab Colorimeter (Color Flex F2, India). The overall color change ( $\Delta E$ ) was calculated by measuring L, a, and b values representing the dried product's lightness/brightness, redness/greenness, and yellowness/blueness, respectively. The extraction of phenolic compounds was done by the method given by Rajoria et al.<sup>[14]</sup> with some modifications. Folin-Ciocalteu spectrophotometric method was used for TPC analysis. The extract was pipetted in an amber color centrifuge tube and Folin Ciocalteu reagent of 0.2 Normality (0.2 N signifies 1 mL of 2 Normality FCR in 10 mL of distilled water) was added followed by addition of sodium carbonate (7.5% w/v). The homogenized mixture was further kept in the dark at ambient for 90 min. The absorbance was measured at 765 nm and the TPC was determined using a standard curve in terms of mgGAE g<sup>-1</sup> of dry material. Specific energy consumption in drying, was estimated as the total energy supplied to the mass of the water evaporated and expressed in kJ kg<sup>-1</sup>.

## 2.7. Quality characterization of MSP powder

FTIR spectra were obtained using FTIR spectrophotometer (Bruker, Alpha E FTIR, Germany). The spectra's transmittance (%) was calculated for a wide range of wavenumber from 4000 to 400 cm<sup>-1</sup>.<sup>[29]</sup> The XRD diffraction patterns were taken using an X-ray diffractometer (Philips PAN analytical, USA). The analysis was done at a five min<sup>-1</sup> scan rate, step size 0.02° in a consistent mode of scanning range between 5° to 75° of 2θ values. Morphology studies were done using FESEM (Nova NanoSEM 450, FEI, USA). Images of the powder were obtained at an electron accelerating voltage of 10–15 kV.<sup>[30]</sup>

## 2.8. Perturbation analysis and optimization

The effect of independent variables on the responses was analyzed by using perturbation plot. A flat line shows the insensitivity of the factor on the response variable whereas the steep line shows the sensitivity of

the response. The Response surface methodology was used to statistically analyze the data, quadratic model was fitted and numerical optimization was done. The drying process was optimized using the numerical optimization technique to find the best combination.

### 3. Results and discussion

#### 3.1. POD and PPO inactivation

POD is the most thermally stable enzyme; consequently, its inactivation results in the deactivation of all other enzymes that are responsible for quality degradation.<sup>[31]</sup> Figure 3 shows the effect of VSPB treatment on POD and PPO activities in Malabar spinach. The POD enzyme's residual activity was higher than the PPO activity. With the increase in treatment time, a significant reduction in the enzyme's activities was observed for all blanching method. After 20 seconds of VSPB treatment, the POD activity was reduced to 15.72%, whereas the PPO activity decreased to 12.04%. However, the POD and PPO activity in HWB was reduced to 32% and 29.80%, respectively after 120 s, while SB resulted in inactivation of POD to 21% and PPO to 18% after 90 s of treatment time. Reduction in the enzyme activity may be due to higher temperature which affects the structure of proteins, rendering them to instability by blocking their active sites.<sup>[25]</sup> The VSPB showed better inactivation of POD and PPO in Malabar spinach compared to SB and HWB. The maximum inactivation was observed at 80 s of treatment time in VSPB, at which the residual activity of POD and PPO was found to be 9.77% and 5.42%, respectively.

The VSPB was finalized because it showed the similar or better result than other literature reported like high hydrostatic pressure blanching of baby

spinach which was performed for the inactivation of POD and PPO activities.<sup>[32]</sup> It took 15 minutes at 700 MPa and 20 °C for the inactivation of the enzymes by 86.4% and 76.7%, respectively. Similarly, Ramesh et al.<sup>[33]</sup> did the inactivation of POD and PPO activity by pulsed microwave blanching of green leafy vegetables and reported that the inactivation was slower, took 125 s to reduce the enzyme activity by 90%. Therefore, VSPB was selected as pretreatment before the drying experiments.

#### 3.2. Effect of infrared power, sample thickness and distance between the emitter and glass plate on quality

The experimental data collected in non-water IR-RWD of MSP are given in Table 2. The moisture content of final product was reduced from 90% (wb) to below 8% (wb). The results of ANOVA (Table S1) showed that *P* and *ST* significantly affected the chlorophyll retention of the MSP whereas non-significant effect was observed when distance between the infrared emitter and glass plate was varied. The proposed quadratic model was highly significant at  $p < 0.01$  and exhibited a non-significant lack of fit at  $p > 0.05$  with  $R^2$  value of 0.957 and adjusted  $R^2$  value of 0.881. The influence of *P*, *ST*, and *D* on the response variable *CR* is shown in the perturbation plot (Figure 4a). The plot illustrates the sensitivity of the *CR* to the process variables. From the plot, it was observed that *P* and *ST* were more responsible for reduction in *CR* than *D*. It may be due to the external forces generated by increased infrared power and subsequent product temperature rise, which might have caused tissue rupture. It resulted to the alterations in chemical and enzymatic processes as well as possible changes in gene expression, which decreased the

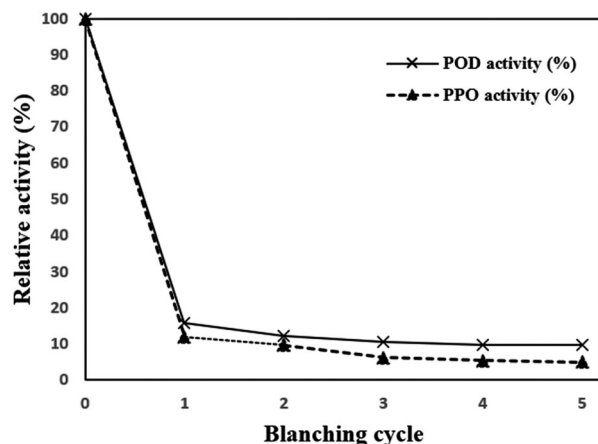
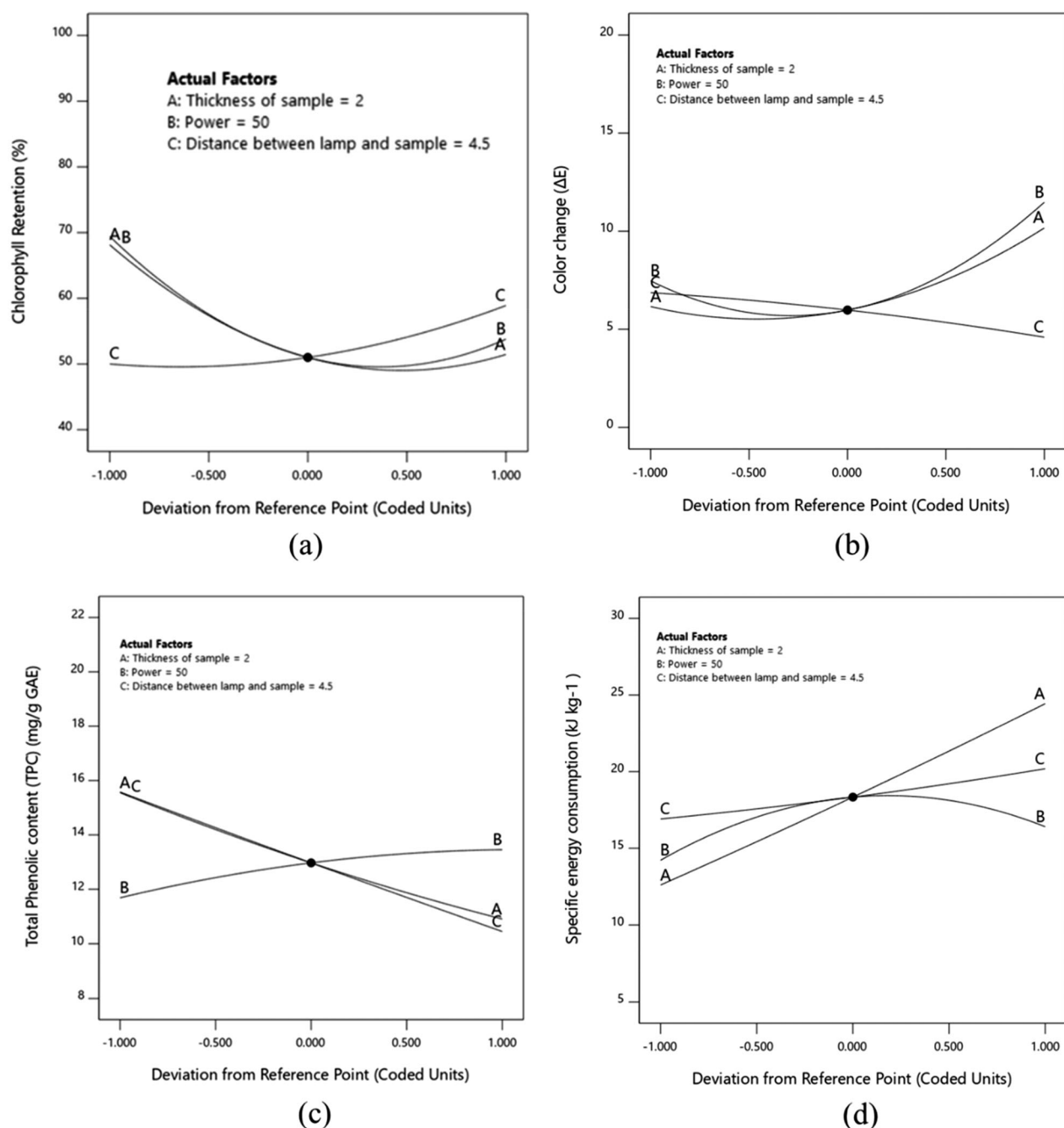


Figure 3. The peroxidase and polyphenol oxidase activity curve during VSPB pretreatment.

Table 2. Actual values of independent variables and experimental data of response.

Expt. No.	ST, mm	P, %	D, cm	CR, %	$\Delta E$	SEC, $\text{kJ kg}^{-1}$	TPC, $\text{mgGAE g}^{-1}$
1	3	30	5.58	76.68	7.33	19.19	9.75
2	2	50	2.4	58.00	9.40	14.98	13.81
3	1	70	5.58	76.20	10.12	14.26	11.18
4	2	50	2.4	53.10	7.10	16.88	17.50
5	2	50	4.5	51.00	5.98	18.34	12.97
6	2	78.28	3.42	61.34	17.70	10.63	16.81
7	3	70	5.58	56.69	13.58	24.50	10.44
8	2	50	2.4	48.70	7.12	16.47	16.51
9	2	50	6.6	64.00	3.90	21.05	9.49
10	0.6	50	3.42	77.99	4.98	8.15	20.61
11	2	50	2.4	43.89	4.78	17.66	19.12
12	1	30	5.58	92.00	11.80	9.17	12.60
13	2	21.72	3.42	80.27	9.60	11.80	11.29
14	3.4	50	3.42	55.68	16.90	27.10	10.11
15	2	50	2.4	54.00	7.00	16.30	16.26



**Figure 4.** The effect of process variables on the responses of MSP during non-water IR-RWD (a) Chlorophyll retention (b) Overall color Change ( $\Delta E$ ) (c) Total phenolic content and (d) Specific energy consumption.

amount of chlorophyll.<sup>[34,35]</sup> The findings agreed with other reported research work on seedless grapes,<sup>[36]</sup> and barley grass powder.<sup>[37]</sup>

The results of ANOVA for  $\Delta E$  in MSP are given in Table S2. It was found that  $ST$  and  $P$  significantly affected the color of the product. The quadratic model was found to be fitted well to the  $\Delta E$  data ( $p < 0.01$ ) with a non-significant lack of fit at  $p > 0.05$ . The  $R^2$  value (0.958) and adjusted  $R^2$  value (0.881) were close to each other resulting in realistic agreement between

them. The influence of  $P$ ,  $ST$ , and  $D$  on  $\Delta E$  is depicted in the perturbation plot in Figure 4b. The  $P$  and  $ST$  was found to be more effective to increase color changes of MSP. The increase in infrared power raises the product temperature causing the variation in  $L$ ,  $a$ ,  $b$  values of the powder leads to increase in the overall color changes. Additionally, increased thickness resulted in prolonged drying time which promote browning that caused reduction in lightness ( $L$ ) value in the MSP.<sup>[38]</sup>



**Table 3.** Coefficients values for all the responses variable with its *p*-values.

Responses	Intercept	A	B	C	AB	AC	BC	A <sup>2</sup>	B <sup>2</sup>	C <sup>2</sup>
CR, %	51.000	−8.338	−7.820	4.447	−1.048	−0.514	−1.566	8.798	10.607	3.452
<i>p</i> -values		0.005*	0.006*	0.030**	0.683	0.838	0.539	0.014**	0.006*	0.265
ΔE	5.980	2.002	2.016	−1.137	1.983	−3.132	−1.213	2.176	3.505	−0.250
<i>p</i> -values		0.0119**	0.0114**	0.0519	0.0421	0.0074**	0.1519	0.0289	0.0042*	0.7760
TPC, mgGAE g <sup>−1</sup>	12.970	−2.324	0.885	−2.564	0.528	1.981	−1.482	0.259	−0.401	0.043
<i>p</i> -values		0.013**	0.209	0.005*	0.570	0.069	0.143	0.773	0.652	0.967
SEC, kJ g <sup>−1</sup>	18.337	5.916	1.095	1.639	0.055	−1.183	2.093	0.181	−3.027	0.212
<i>p</i> -values		< .0001*	0.017**	0.002*	0.905	0.041**	0.005*	0.691	0.001*	0.689

\*1% Level of significance.

\*\*5% Level of significance.

The total phenolic content of MSP ranged from 7.79 to 19.11 mgGAE g<sup>−1</sup>. The proposed quadratic model was highly significant at  $p < 0.01$  exhibited a non-significant lack of fit at  $p > 0.05$  with R<sup>2</sup> value (0.919) and adjusted R<sup>2</sup> value (0.773) respectively. The ANOVA (Table S3) results revealed that, the *ST* and *P* significantly affect the *TPC* content. Distance between the emitter and glass plate showed a positive effect on *TPC*, as the retention of *TPC* was seem to be more if the distance is increased. This may be due delaying of diffusion of heat into the sample. The maximum retention of the total phenolic compound was around 70% to the fresh weight. It may be due to lesser rise in the product temperature (around 75 °C) during drying, as well as the inactivation of polyphenol oxidase enzyme prior to processing which is one of the leading causes of degradation of phenolic compounds during long-time drying procedures.<sup>[39,40]</sup> The perturbation graph for the total phenolic content is shown in Figure 4c. From the plot it is apparent that the *TPC* is highly sensitive to *ST* and *D*.

The ANOVA result for specific energy consumption in drying of MSP are given in Table S4. It was found that all process variables significantly affected the *SEC*. The quadratic model was found to be fitted well to the energy consumption data ( $p < 0.01$ ) with a non-significant lack of fit at  $p > 0.05$  with the R<sup>2</sup> value (0.990) and adjusted R<sup>2</sup> value (0.973). The influence of *P*, *ST*, and *D* on specific energy consumption is depicted in the perturbation plot in Figure 4d. The plot shows that the *ST* was more responsible for increase in energy consumption. The energy consumption was increased with an increase in thickness of sample whereas the decrease in energy consumption was recorded with rise in *P*. It was because with the increase in power, the product temperature rise, leading to faster removal of water in lesser drying time, therefore lowers *SEC*.<sup>[13]</sup> The coefficients table for all the responses variable is shown in Table 3.

### 3.3. Process optimization

The numerical optimization for drying of MSP using non water IR-RWD was done by keeping *P*, *ST* and *D* in the range with aim of MSP having maximum chlorophyll retention, total phenolic content, minimum color change and lower specific energy consumption. The design expert software gave optimum conditions at 40% *P*, 1.2 mm *ST* and 3.67 cm *D* with a desirability value of 0.92. The dependent variables at optimum condition were 67.38% *CR*, 7.715 ΔE, 11.2 kJ kg<sup>−1</sup> *SEC* and 16.57 mgGAE g<sup>−1</sup> *TPC*.

### 3.4. Drying characteristics of MSP during non-water IR-RWD

The variation in the moisture content over drying time is illustrated in Figure 5a. The drying time decreased as the intensity of infrared power increased from 150 W to 350 W. In contrast, increased *ST* and *D* resulted in a slower removal of moisture content, thereby increasing the drying time. The moisture removal was faster for 1 mm *ST*, 70% *P* and 5.58 cm *D*, which dried product in 20 min. This was because when a sample was exposed to infrared energy with higher intensity, the vibration between the water molecules increases, resulting in fast heating of the surface and inner layer. As a result, the internal pressure of the water vapor increased, which accelerated the moisture migration from inside to outside, resulting in water evaporation with time.<sup>[26,41]</sup> *P*, *ST* and *D* all together showed a significant role in moisture removal of MSP and reducing the drying time of the product. The results were consistent with previous observations of other products being dried, including apricot pomace,<sup>[42]</sup> and Blue mussels.<sup>[43]</sup>

Generally, agricultural commodities drying occurs in falling rate periods.<sup>[44]</sup> According to Figure 5b, the drying rate showed a nonlinear pattern in all the process conditions. With an increase in the intensity of

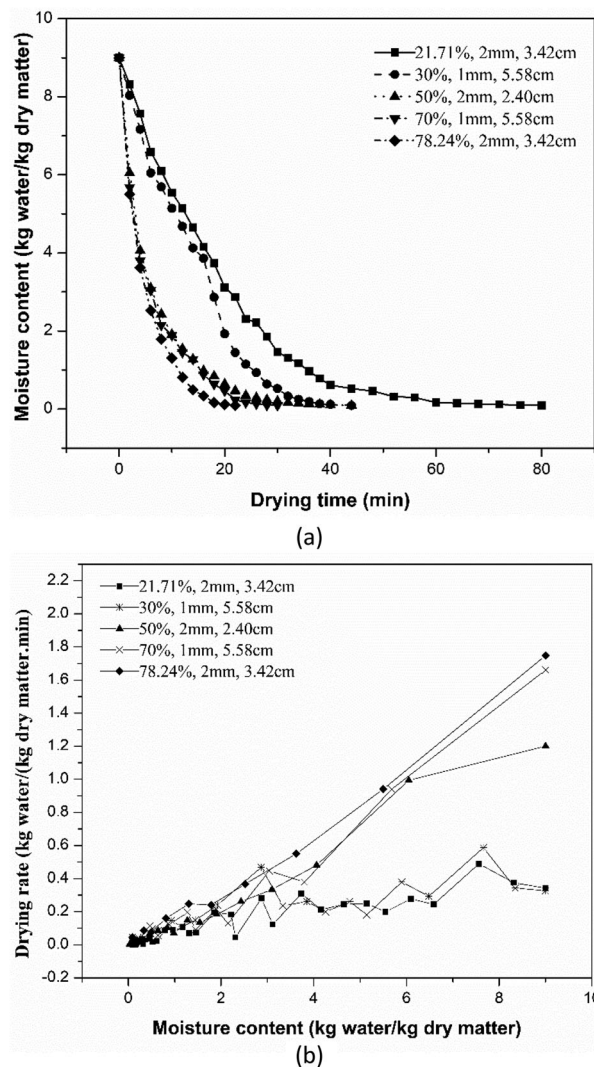


**Figure 5.** Variation in moisture content with drying time – curve (a), and drying rate over moisture content – curve (b) of non-water IR-RWD.

power (150 W to 350 W), the internal water vapor pressure increased, resulting in more pores opening in the sample and faster moisture removal. As a result, the drying rate increases incrementally as the  $P$  increased. Also, it was noticed that drying rates were higher during initial period of time and gradually decreased as the process progressed. The similar phenomenon was used to be observed in traditional RWD. It is because at the beginning the moisture content of the product is high leading to more generation of the heat into the sample. It results in the rapid heating of the product whereas in the later stages the moisture content of the product decreased, therefore the heat penetration reduces and the evaporation of moisture from the surface becomes less. A similar observation was reported for infrared drying of kiwifruit [45] and, black mulberry. [46]

**Table 4.** Page model constants and moisture diffusivity values during non-water IR-RWD.

Exp. No.	$ST$ , mm	$P$ , %	$D$ , cm	Page model			$D$ , $m^2 s^{-1}$
				$k$ ( $min^{-1}$ )	$n$	$R^2$	
1	3	30	5.58	0.0227	1.242	0.995	$3.816 \times 10^{-8}$
2	2	50	2.4	0.2482	0.823	0.998	$5.852 \times 10^{-8}$
3	1	70	5.58	0.2682	0.805	0.996	$1.774 \times 10^{-8}$
4	2	50	2.4	0.2399	0.813	0.998	$5.853 \times 10^{-8}$
5	2	50	4.5	0.0829	1.101	0.994	$3.518 \times 10^{-8}$
6	2	78.28	3.42	0.0224	1.245	0.991	$7.396 \times 10^{-8}$
7	3	70	5.58	0.0733	1.028	0.997	$6.626 \times 10^{-8}$
8	2	50	2.4	0.2499	0.824	0.998	$5.712 \times 10^{-8}$
9	2	50	6.6	0.0164	1.429	0.981	$2.538 \times 10^{-8}$
10	0.6	50	3.42	0.2302	0.923	0.997	$7.396 \times 10^{-8}$
11	2	50	2.4	0.2471	0.822	0.998	$5.853 \times 10^{-8}$
12	1	30	5.58	0.0214	1.387	0.990	$6.845 \times 10^{-9}$
13	2	21.72	3.42	0.0303	1.197	0.997	$1.609 \times 10^{-8}$
14	3.4	50	3.42	0.0593	1.079	0.997	$3.271 \times 10^{-8}$
15	2	50	2.4	0.2312	0.813	0.998	$5.613 \times 10^{-8}$

### 3.5. Modeling drying kinetics and apparent moisture diffusivity

The infrared power, sample thickness and distance were significantly responsible for variation in moisture ratio with time of MSP. The drying curves showed a quick decline achieving moisture ratio equilibrium in a shorter time; the same phenomena occurred in traditional RWD. The Page model data are given in Table 4. The  $R^2$  values for the Page model were between 0.991–0.998, and RMSE were 0.0017–0.041 indicating its suitability to the drying data. The value of  $k$  increased as the intensity of infrared radiation increase; hence, infrared radiation was found to be advantageous for accelerating the drying rate whereas, with increased in  $ST$  and  $D$ , the  $k$  value was decreased. The page model constant ( $n$ ) value varied from 0.805–1.429 showed the diffusion occurred during the non-water IR-RWD. [31]

The  $D$  values for non-water IR-RWD at different process variables are given in Table 4. The calculated values of the effective moisture diffusivity ranged from  $1.609 \times 10^{-8}$  to  $6.845 \times 10^{-9} m^2 s^{-1}$ , respectively. With increased in  $P$ , the diffusivity was also increased. Higher infrared intensity might have enhanced the molecular vibration, electronic states, and rotation of atoms which lead to rise in the product temperature and vapor pressure thus accelerating the movement of moisture toward the sample surface. [26] The other researchers published similar results for a variety of commodities like sweet potato, [47] mushroom slices [48] dried using infrared or infrared assisted drying.

### 3.6. Effect of infrared power, sample thickness and distance on mass transfer parameters of MSP

The mass transfer coefficients  $S$  and  $J$  and the model fitting criteria ( $R^2$ , and RMSE) are given in Table 5.

The lower RMSE and the higher  $R^2$  values indicate the successful model fitting. The  $S$  indicate the sample's drying capacity per unit time and it has a direct impact on moisture diffusivity.<sup>[49]</sup> The  $S$  values were varied from 8.62 to  $96.5\text{ s}^{-1}$  which was similar to blueberry pulp dried using refractance and hot air drying.<sup>[50]</sup> From the perturbation plot (Figure 6a) it can be observed that, the process variables significantly affected the drying coefficients. The increase in  $P$  and decrease in  $ST$  and  $D$ , the  $S$  value increased. The increase in power causes more collisions between the molecules; resulting in enough energy acquired by the water molecules leading to faster movement toward the surface of the sample and therefore, increases the drying capacity of the sample.<sup>[50]</sup> So, this was the unique advantage of an infrared radiation.

The lag factor ( $J$ ), which is a function of the Biot number, indicates the amount of the internal and

external resistance to the moisture transfer from the sample. The lag factor for the Malabar spinach paste varied from 1.001 to 1.091 that was similar to lag factor reported for passion fruit peel dried using tray drier.<sup>[51]</sup> The  $J$  value greater than 1 indicating the Biot number was in the range of 0 to 100 which signified the involvement of both internal and external resistance in moisture diffusivity. The  $B_i$  values estimated in all experiments were close to 0.1. Similar range was mentioned by other researchers for products like apple slices<sup>[14]</sup> and passion fruit peel.<sup>[51]</sup> From Table 6 it can be observed that the  $B_i$  is differentiated in two groups;  $B_i < 0.1$  indicates that major effect on mass diffusivity is due to the external resistance (internal resistance is almost negligible) and  $0.1 > B_i < 100$  signifies internal and external resistances are comparable and have a finite value. The moisture diffusivity ( $D_a$ ) and moisture transfer coefficients ( $h_m$ ) were calculated

**Table 5.** Mass transfer and model statistical parameters obtained during non-water IR RWD.

Expt. No.	$ST$ , mm	$P$ , %	$D$ , cm	$S$ , $\text{s}^{-1}$	$J$	$R^2$	RMSE
1	3	30	5.58	6.71	1.067	0.987	0.036
2	2	50	2.4	49.3	1.018	0.991	0.010
3	1	70	5.58	61.4	1.011	0.986	0.014
4	2	50	2.4	47.5	1.013	0.991	0.010
5	2	50	4.5	26.8	1.045	0.994	0.011
6	2	78.28	3.42	52.2	1.068	0.983	0.054
7	3	70	5.58	17.5	1.012	0.997	0.005
8	2	50	2.4	47.4	1.012	0.991	0.010
9	2	50	6.6	13.1	1.091	0.957	0.110
10	0.6	50	3.42	99.8	1.013	0.996	0.003
11	2	50	2.4	47.9	1.011	0.991	0.010
12	1	30	5.58	22.1	1.088	0.969	0.068
13	2	21.72	3.42	10.9	1.051	0.991	0.022
14	3.4	50	3.42	13.3	1.031	0.997	0.007
15	2	50	2.4	45.2	1.012	0.991	0.010

**Table 6.** Biot number, and moisture diffusivity obtained during non-water IR RWD.

Expt. No.	$ST$ , mm	$P$ , %	$D$ , cm	$B_i$	$h_m$ , $\text{m s}^{-1}$	$D_a$ , $\text{m}^2 \text{ s}^{-1}$
1	3	30	5.58	0.447	$10.43 \times 10^{-7}$	$6.997 \times 10^{-9}$
2	2	50	2.4	0.098	$23.2 \times 10^{-7}$	$53.53 \times 10^{-9}$
3	2	50	2.4	0.058	$17.17 \times 10^{-7}$	$29.27 \times 10^{-9}$
4	2	50	2.4	0.070	$17.3 \times 10^{-7}$	$51.13 \times 10^{-9}$
5	1	70	5.58	0.273	$29.28 \times 10^{-7}$	$21.42 \times 10^{-9}$
6	2	50	2.4	0.456	$21.11 \times 10^{-7}$	$92.75 \times 10^{-9}$
7	2	50	4.5	0.064	$7.094 \times 10^{-7}$	$33.12 \times 10^{-9}$
8	2	50	2.4	0.064	$16.47 \times 10^{-7}$	$51.27 \times 10^{-9}$
9	2	78.28	3.42	0.681	$52.71 \times 10^{-7}$	$15.48 \times 10^{-9}$
10	3	70	5.58	0.069	$17.45 \times 10^{-7}$	$14.99 \times 10^{-9}$
11	2	50	2.4	0.064	$15.7 \times 10^{-7}$	$51.34 \times 10^{-9}$
12	2	50	2.4	0.648	$58.09 \times 10^{-7}$	$8.951 \times 10^{-9}$
13	2	50	6.6	0.317	$6.69 \times 10^{-7}$	$4.21 \times 10^{-9}$
14	0.6	50	3.42	0.178	$11.99 \times 10^{-7}$	$22.89 \times 10^{-9}$
15	2	50	2.4	0.059	$16.8 \times 10^{-7}$	$48.01 \times 10^{-9}$

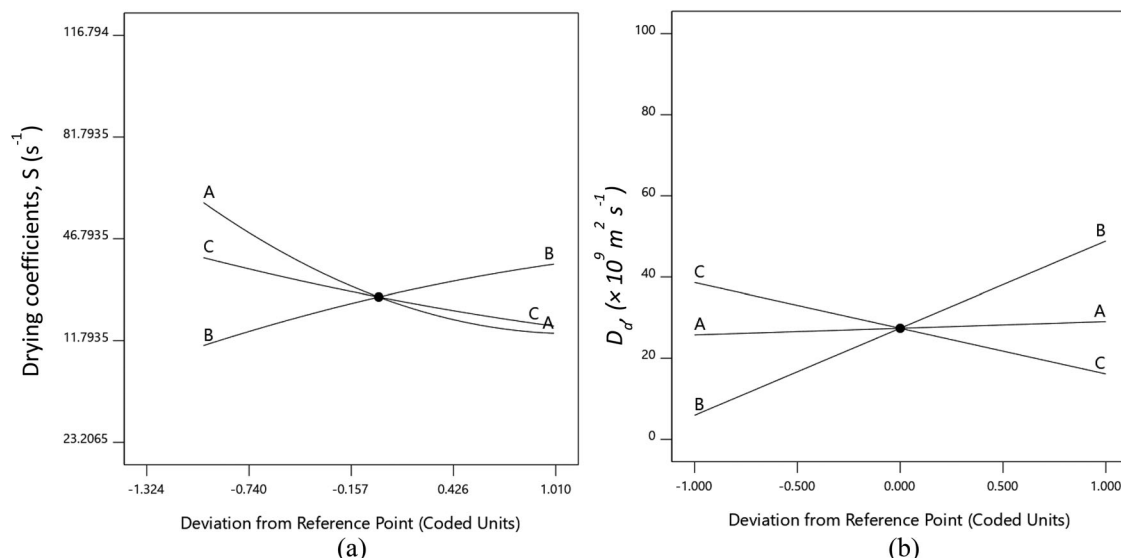


**Figure 6.** Perturbation analysis of drying coefficients and effective moisture diffusivity during non-water IR-RWD process.



using Eq. (14). The value of  $D_a$  and  $h_m$  were in the range between  $4.21 \times 10^{-9}$  to  $92.5 \times 10^{-9} \text{ m}^2 \text{ s}^{-1}$ , and  $6.6 \times 10^{-7} \text{ m s}^{-1}$  to  $58.09 \times 10^{-7}$  respectively. Figure 6b showed the perturbation plot of moisture diffusivity. It was observed that  $D_a$  increased with power, and decreased with sample thickness and distance. This signified that in most cases the internal resistance shows significant effect.<sup>[50]</sup>

### 3.7. FTIR analysis

The FTIR spectra of the optimized MSP by IR-RWD and MSP by traditional RWD was recorded to identify the presence of functional groups. In both cases similar spectra was found and shown in Figure 7a,b. A broad-band at around  $3267 \text{ cm}^{-1}$  was attributed stretching vibration of surface adsorbed moisture in the form of intermolecular bonded hydroxyl group. The peaks at around  $2918$  and  $2857 \text{ cm}^{-1}$  were assigned to the symmetric and asymmetric stretching vibration of C-H band and stretching vibration of N-H band, correspond to both alkyl and aromatic group, respectively.<sup>[29,30,52]</sup> Further, the band at  $1727$  and  $1631 \text{ cm}^{-1}$  were attributed to the stretching vibration of C=O band and C=C band in benzene ring respectively. In fingerprint region from  $1500 \text{ cm}^{-1}$  to

$700 \text{ cm}^{-1}$ , the band at  $1319$  and  $1221 \text{ cm}^{-1}$  was assigned to the bending vibration of C-H and C-N band, often belong to aromatic secondary amine and carotenes respectively.<sup>[53]</sup> The intense strong band at  $1021 \text{ cm}^{-1}$  corresponded to the stretching vibration of C-O band of oligosaccharides functional group.<sup>[54,55]</sup> The band at around  $846$  and  $786 \text{ cm}^{-1}$  was attributed to the C-H bending vibration of benzene ring isoprenoid,<sup>[52]</sup> respectively.

### 3.8. XRD analysis

X-ray Diffraction (XRD) was used for phase analysis of material. The XRD patterns of the optimized MSP by IR-RWD and MSP by traditional RWD are shown in Figure 8a,b, respectively. Both diffraction pattern showed a crystalline peaks at angles ( $2\theta$ ) =  $15.12$ ,  $18.18$ , and  $24.33$  conforming beta carotene phase are present.<sup>[56]</sup> The crystalline peak intensity was found to be little higher in non-water IR- RWD than the peak of traditional RWD which indicates atoms are in periodic manners in optimized MSP<sub>IR-RWD</sub>. The broad hump in the range of  $2\theta = 20$  to  $25^\circ$ , that specified a semi crystalline nature and indicates the domain of ascorbic acid.<sup>[57]</sup> Another crystalline peak at angles  $2\theta = 30.49$ ,  $36.30$ , and  $38.44$  confirms magnesium

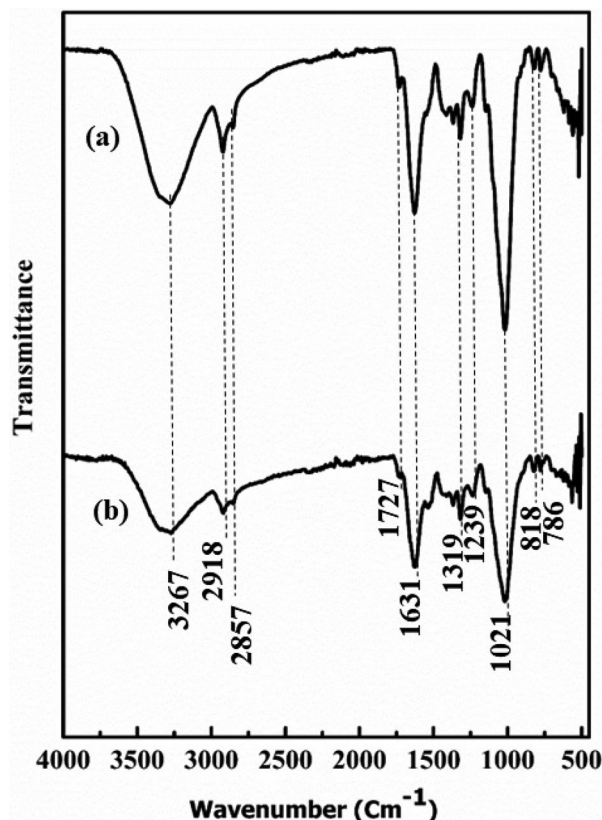


**Figure 7.** FTIR spectra of dried powder optimized MSP by IR-RWD – curve (a); and MSP traditional RWD – curve (b).

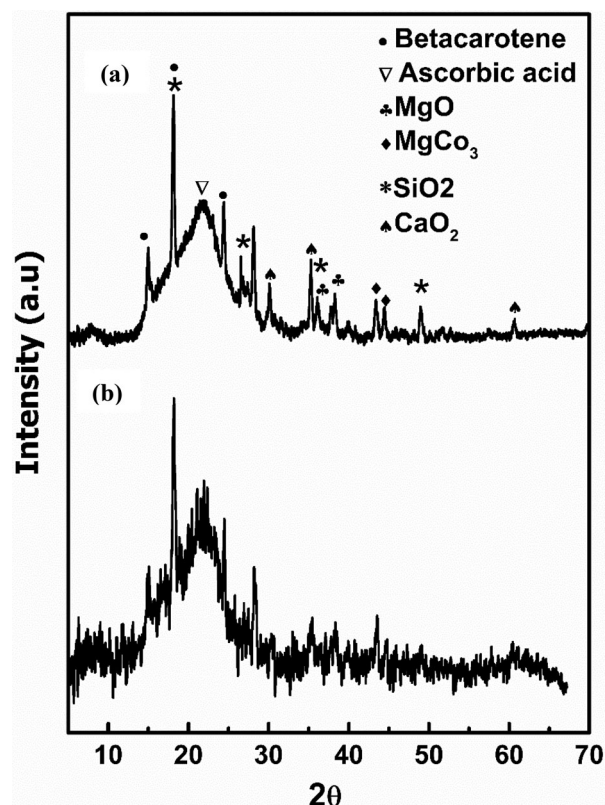


**Figure 8.** XRD analysis of dried powder optimized MSP by IR-RWD – curve (a); and MSP traditional RWD – curve (b).

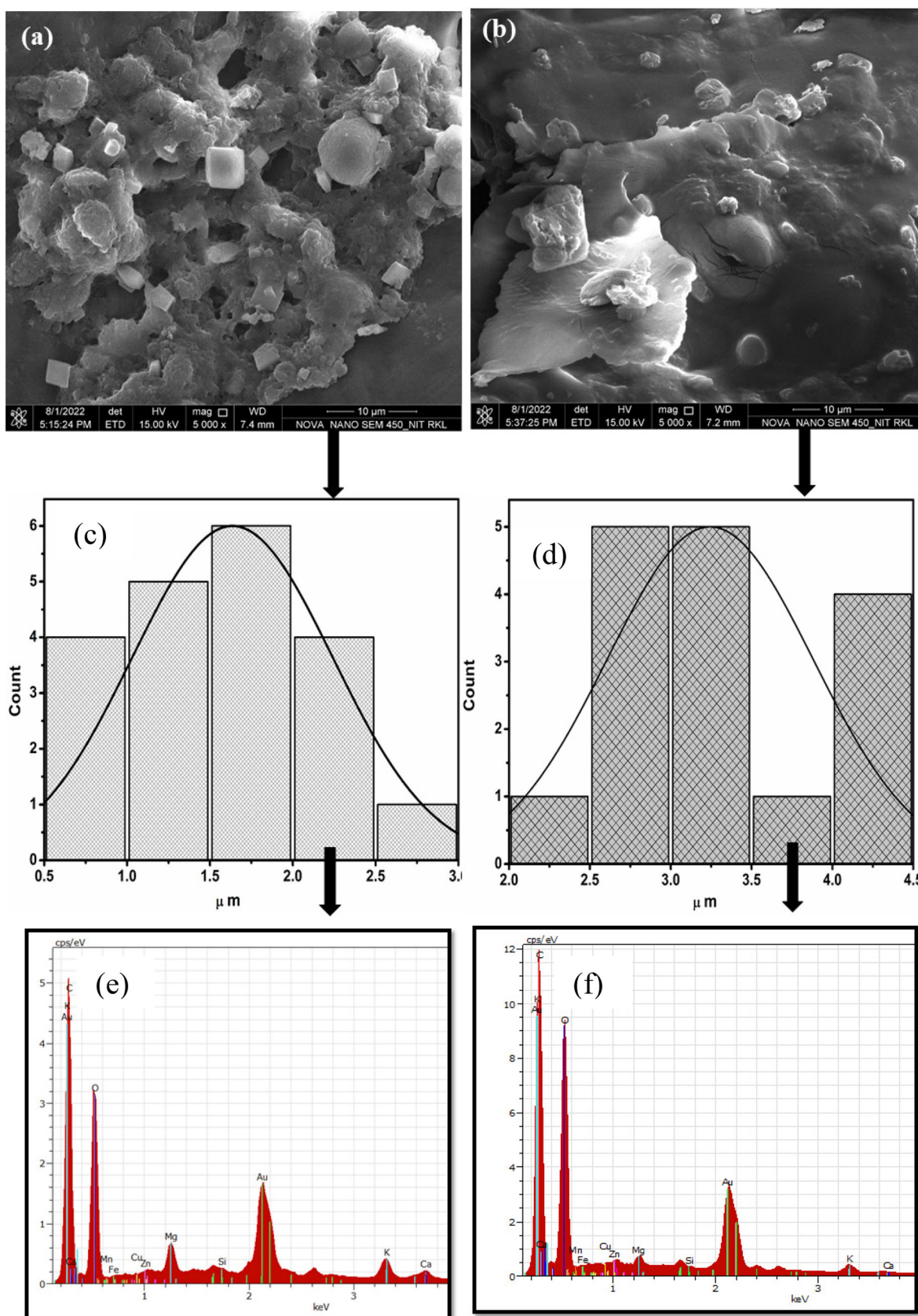


**Figure 9.** FESEM analysis of optimized MSP by IR-RWD – curve (a); MSP by RWD – curve (b); Particle size distribution optimized MSP by IR-RWD – curve (c); MSP by RWD – curve (d); EDS analysis of optimized MSP by IR-RWD – curve (e); MSP by RWD – curve (f).



**Table 7.** Elemental composition in optimized MSP by IR-RWD and traditional MSP by RWD.

Element	Optimized non-water IR-RWD		Traditional RWD	
	Normal wt., %	Atomic wt., %	Normal wt., %	Atomic wt., %
Oxygen	49.58	45.50	50.47	45.52
Carbon	41.36	50.57	42.95	51.60
Potassium	3.70	1.39	2.68	0.99
Magnesium	1.50	0.91	2.20	1.31
Chlorine	1.46	0.61	0.00	0.00
Sodium	0.87	0.56	0.00	0.00
Copper	0.68	0.16	0.24	0.06
Calcium	0.58	0.21	1.36	0.49
Silicon	0.12	0.06	0.08	0.08
Manganese	0.10	0.03	0.00	0.00
Iron	0.04	0.01	0.00	0.00

oxide;  $2\theta = 43.18$  and  $44.67$  magnesium carbonate;  $2\theta = 30.06$ ,  $35.43$ , and  $60.82$  calcium peroxide; and  $2\theta = 18.23$ ,  $26.83$ ,  $36.30$  and  $49.20$  silica oxide were present in dried Malabar spinach powder.<sup>[58]</sup>

### 3.9. FESEM analysis

Particle morphology and elemental composition of optimized MSP by IR-RWD and MSP by traditional RWD was investigated using FESEM and EDS analysis. In Figure 9a–d, square shape agglomerated porous like morphology with particle size in the range of 2 to 3 micrometers was observed in optimized MSP by IR-RWD whereas highly agglomerated irregular shape like morphology with particle size range of 2 to 5 micrometer was observed in case of traditional MSP. The particle size of MSP by non-water IR-RWD was found to be smaller than traditional RWD dried MSP.

The EDS showed in Figure 9e,f clearly indicated the presence of several elements like carbon, oxygen, potassium, calcium, magnesium, Iron, sodium, and chlorine at different proportions in the dried MSP (Table 7). The presence of identified elements in non-water IR-RWD dried MSP will be beneficial for the human body, such as calcium is required for building up bones and helps in blood coagulation, potassium ions being used for transportation of glucose in the muscle fibers, magnesium another important element for the development of bone and helps in repairing of injured cells, chlorine helps in maintain the pH in the stomach and iron aids in prevention of anemia.<sup>[59]</sup>

## 4. Conclusions

The non-water IR-RWD method is an efficient and prominent alternative to traditional RWD. It takes  $1/3^{\text{rd}}$  times lower drying time than traditional RWD because of absence of water heating process. The non-

water IR-RWD models fitted to the data collected by using the hybrid experimental design effectively predicted the response. The sample thickness, infrared power and distance between the emitter and glass plate showed a significant influence on the quality characteristics of Malabar spinach powder. The optimum conditions were obtained to be 40% (0.2 kW) infrared power, 1.2 mm sample thickness, and 3.67 cm distance between the infrared emitter and glass plate. The Page model showed the best fit to the drying kinetics, and IR power enhanced drying rate and moisture diffusivity. Also, mass transfer analysis showed a greater drying capacity in non-water IR-RWD. From the quality characterization study, the FTIR spectra for both optimized MSP by IR-RWD and RWD showed the similar pattern indicating the presence of functional groups. The semi-crystalline phase with a square shape agglomerated porous like morphology was observed in optimized MSP by non-water IR-RWD whereas highly agglomerated porous like morphology of dried powder was observed in traditional RWD. There is a future scope for using large-sized toughened glass plates in the development of batch-type IR-RWD dryers, as toughened glass plates are extensively used in solar cabinet dryers.

## Disclosure statement

No potential conflict of interest was reported by the author(s).

## Funding

The authors are thankful to Science and Engineering Board (India) [Grant Number IMP/2018/002120] for providing facilities to this research work.

## ORCID

Parag Prakash Sutar  <http://orcid.org/0000-0002-1018-382X>

## References

- [1] Sarkar, T.; Salauddin, M.; Roy, S.; Chakraborty, R.; Rebezov, M.; Shariati, M. A.; Thiruvengadam, M.; Rengasamy, K. R. R. Underutilized Green Leafy Vegetables: Frontier in Fortified Food Development and Nutrition. *Crit. Rev. Food Sci. Nutr.* **2022**, 1–55. DOI: [10.1080/10408398.2022.2095555](https://doi.org/10.1080/10408398.2022.2095555).
- [2] Karwacka, M.; Ciurzyńska, A.; Galus, S.; Janowicz, M. Freeze-Dried Snacks Obtained from Frozen Vegetable by-Products and Apple Pomace – Selected Properties, Energy Consumption and Carbon

- Footprint. *Innov. Food Sci. Emerg. Technol.* **2022**, 77, 102949. DOI: [10.1016/j.ifset.2022.102949](https://doi.org/10.1016/j.ifset.2022.102949).
- [3] Rajkumar, G.; Rajan, M.; Araujo, H. C.; Jesus, M. S.; Leite Neta, M. T. S.; Sandes, R. D. D.; Narain, N. Comparative Evaluation of Volatile Profile of Tomato Subjected to Hot Air, Freeze, and Spray Drying. *Dry. Technol.* **2021**, 39, 383–391. DOI: [10.1080/07373937.2020.1842441](https://doi.org/10.1080/07373937.2020.1842441).
- [4] Singh, A.; Dubey, P. K.; Chaurasiya, R.; Mathur, N.; Kumar, G.; Bharati, S.; Abhilash, P. C. Indian Spinach: An Underutilized Perennial Leafy Vegetable for Nutritional Security in Developing World. *Energ. Ecol. Environ.* **2018**, 3, 195–205. DOI: [10.1007/s40974-018-0091-1](https://doi.org/10.1007/s40974-018-0091-1).
- [5] Putriani, N.; Perdana, J.; Nugraheni, P. Y. Effect of Thermal Processing on Key Phytochemical Compounds in Green Leafy Vegetables: A Review. *Food Rev. Int.* **2020**, 38, 783–811. DOI: [10.1080/87559129.2020.1745826](https://doi.org/10.1080/87559129.2020.1745826).
- [6] Shivanna, V. B.; Subban, N. Effect of Various Drying Methods on Flavor Characteristics and Physicochemical Properties of Dried Curry Leaves (*Murraya koenigii* L. spreng). *Dry. Technol.* **2014**, 32, 882–890. DOI: [10.1080/07373937.2013.871727](https://doi.org/10.1080/07373937.2013.871727).
- [7] Yamakage, K.; Yamada, T.; Takahashi, K.; Takaki, K.; Komuro, M.; Sasaki, K.; Aoki, H.; Kamagata, J.; Koide, S.; Orikasa, T. Impact of Pre-Treatment with Pulsed Electric Field on Drying Rate and Changes in Spinach Quality during Hot Air Drying. *Innov. Food Sci. Emerg. Technol.* **2021**, 68, 102615. DOI: [10.1016/j.ifset.2021.102615](https://doi.org/10.1016/j.ifset.2021.102615).
- [8] Asimwe, A.; Kigozi, J. B.; Baidhe, E.; Muyonga, J. H. Optimization of Refractance Window Drying Conditions for Passion Fruit Puree. *LWT* **2022**, 154, 112742. DOI: [10.1016/j.lwt.2021.112742](https://doi.org/10.1016/j.lwt.2021.112742).
- [9] Hernández-Santos, B.; Martínez-Sánchez, C. E.; Torruco-Uco, J. G.; Rodríguez-Miranda, J.; Ruiz-López, I. I.; Vajando-Anaya, E. S.; Carmona-García, R.; Herman-Lara, E. Evaluation of Physical and Chemical Properties of Carrots Dried by Refractance Window Drying. *Dry. Technol.* **2016**, 34, 1414–1422. DOI: [10.1080/07373937.2015.1118705](https://doi.org/10.1080/07373937.2015.1118705).
- [10] Santos, S. d J. L.; Canto, H. K. F.; da Silva, L. H. M.; Rodrigues, A. M. d C. Characterization and Properties of Purple Yam (*Dioscorea trifida*) Powder Obtained by Refractance Window Drying. *Dry. Technol.* **2022**, 40, 1103–1113. DOI: [10.1080/07373937.2020.1847140](https://doi.org/10.1080/07373937.2020.1847140).
- [11] Castoldi, M.; Zotarelli, M. F.; Durigon, A.; Carciofi, B. A. M.; Laurindo, J. B. Production of Tomato Powder by Refractance Window Drying. *Dry. Technol.* **2015**, 33, 1463–1473. DOI: [10.1080/07373937.2014.989327](https://doi.org/10.1080/07373937.2014.989327).
- [12] Vargas, L.; Kapoor, R.; Nemzer, B.; Feng, H. Application of Different Drying Methods for Evaluation of Phytochemical Content and Physical Properties of Broccoli, Kale, and Spinach. *LWT* **2022**, 155, 112892. DOI: [10.1016/j.lwt.2021.112892](https://doi.org/10.1016/j.lwt.2021.112892).
- [13] Deepika, S.; Sutar, P. P. Combining Osmotic–Steam Blanching with Infrared–Microwave–Hot Air Drying: Production of Dried Lemon (*Citrus limon* L.) Slices and Enzyme Inactivation. *Dry. Technol.* **2018**, 36, 1719–1737. DOI: [10.1080/07373937.2017.1422744](https://doi.org/10.1080/07373937.2017.1422744).
- [14] Rajoriya, D.; Shewale, S. R.; Bhavya, M. L.; Hebbar, H. U. Far Infrared Assisted Refractance Window Drying of Apple Slices: Comparative Study on Flavour, Nutrient Retention and Drying Characteristics. *Innov. Food Sci. Emerg. Technol.* **2020**, 66, 102530. DOI: [10.1016/j.ifset.2020.102530](https://doi.org/10.1016/j.ifset.2020.102530).
- [15] Tontul, I.; Eroğlu, E.; Topuz, A. Convective and Refractance Window Drying of Cornelian Cherry Pulp: Effect on Physicochemical Properties. *J. Food Process. Eng.* **2018**, 41, e12917–8. DOI: [10.1111/jfpe.12917](https://doi.org/10.1111/jfpe.12917).
- [16] Puente, L.; Vega-Gálvez, A.; Ah-Hen, K. S.; Rodríguez, A.; Pasten, A.; Poblete, J.; Pardo-Orellana, C.; Muñoz, M. Refractance Window Drying of Goldenberry (*Physalis peruviana* L.) Pulp: A Comparison of Quality Characteristics with Respect to Other Drying Techniques. *LWT* **2020**, 131, 109772. DOI: [10.1016/j.lwt.2020.109772](https://doi.org/10.1016/j.lwt.2020.109772).
- [17] Shende, D.; Datta, A. K. Refractance Window Drying of Fruits and Vegetables: A Review. *J. Sci. Food Agric.* **2019**, 99, 1449–1456. DOI: [10.1002/jsfa.9356](https://doi.org/10.1002/jsfa.9356).
- [18] Abul-Fadl, M. M.; Ghanem, T. H. Effect of Refractance-Window (RW) Drying Method on Quality Criteria of Produced Tomato Powder as Compared to the Convection Drying Method. *World Appl. Sci. J.* **2011**, 15, 953–965.
- [19] Tran, D. Q. Effects of Drying Methods on Color Retention and Chlorophyll of Celery (*Apium graveolens* L.), Spinach (*Spinacia oleracea* L.), Malabar Spinach (*Basella alba* L.). *J. Agric. Dev.* **2021**, 19, 53–61. DOI: [10.52997/jad.6.06.2020](https://doi.org/10.52997/jad.6.06.2020).
- [20] Sahin, F. H.; Acikgoz, F. E.; Eremkere, M.; Aktas, T. Physical and Mechanical Properties and Influence of Drying Techniques on Drying Characteristics and Some Quality Parameters of Malabar Spinach (*Basella alba* L.). *Fresenius Environ. Bull.* **2019**, 28, 4340–4352.
- [21] Association of Official Agricultural Chemists. *Official Methods of Analysis*. AOAC: Washington, DC, **1990**.
- [22] Wang, H.; Meng, J. S.; Raghavan, G. S. V.; Orsat, V.; Yu, X. L.; Liu, Z. L.; Zheng, Z. A.; Wang, S. Y.; Xiao, H. W. Vacuum-Steam Pulsed Blanching (VSPB) Enhances Drying Quality, Shortens the Drying Time of Ginger by Inactivating Enzymes, Altering Texture, Microstructure and Ultrastructure. *LWT* **2022**, 154, 112714. DOI: [10.1016/j.lwt.2021.112714](https://doi.org/10.1016/j.lwt.2021.112714).
- [23] Wang, H.; Fang, X. M.; Sutar, P. P.; Meng, J. S.; Wang, J.; Yu, X. L.; Xiao, H. W. Effects of Vacuum-Steam Pulsed Blanching on Drying Kinetics, Colour, Phytochemical Contents, Antioxidant Capacity of Carrot and the Mechanism of Carrot Quality Changes Revealed by Texture, Microstructure and Ultrastructure. *Food Chem.* **2021**, 338, 127799. DOI: [10.1016/j.foodchem.2020.127799](https://doi.org/10.1016/j.foodchem.2020.127799).
- [24] Zhang, Y.; Sun, B. H.; Pei, Y. P.; Vidyarthi, S. K.; Zhang, W. P.; Zhang, W. K.; Ju, H. Y.; Gao, Z. J.; Xiao, H. W. Vacuum-Steam Pulsed Blanching (VSPB): An Emerging Blanching Technology for Beetroot. *LWT* **2021**, 147, 111532. DOI: [10.1016/j.lwt.2021.111532](https://doi.org/10.1016/j.lwt.2021.111532).

- [25] Kar, S.; Sutar, P. P. Enhancing the Efficacy of Microwave Blanching-Cum-Black Mould Inactivation of Whole Garlic (*Allium sativum* L.) Bulbs Using Ultrasound: Higher Inactivation of Peroxidase, Polyphenol Oxidase, and *Aspergillus niger* at Lower Processing Temperatures. *Food Bioproc. Tech.* **2022**, *15*, 635–655. DOI: [10.1007/s11947-022-02769-5](https://doi.org/10.1007/s11947-022-02769-5).
- [26] Delfiya, D. S. A.; Prashob, K.; Murali, S.; Alfiya, P. V.; Samuel, M. P.; Pandiselvam, R. Drying Kinetics of Food Materials in Infrared Radiation Drying. A Review. *J. Food Process. Eng.* **2022**, *45*, 1–19. DOI: [10.1111/jfpe.13810](https://doi.org/10.1111/jfpe.13810).
- [27] Dincer, I.; Dost, S. A Modelling Study for Moisture Diffusivities and Moisture Transfer Coefficients in Drying of Solid Objects. *Int. J. Energy Res.* **1996**, *20*, 531–539. DOI: [10.1002/\(SICI\)1099-114X\(199606\)20:6<531::AID-ER171>3.0.CO;2-6](https://doi.org/10.1002/(SICI)1099-114X(199606)20:6<531::AID-ER171>3.0.CO;2-6).
- [28] Sadasivam, S.; Manickam, A. *Biochemical Methods*, 3rd ed.; New Age International (Pvt) Ltd: New Delhi, India, **2009**; pp. 7–18.
- [29] Singh Yadav, B.; Kumar Sahu, R.; Kumar Pramanick, A.; Mishra, T.; Alam, A.; Bharti, M.; Mukherjee, S.; Kumar, S.; Nayar, S. Collagen Functionalized Graphene Sheets Decorated with in Situ Synthesized Nano Hydroxyapatite Electrospun into Fibers. *Mater. Today Commun.* **2019**, *18*, 167–175. DOI: [10.1016/j.mtcomm.2018.11.005](https://doi.org/10.1016/j.mtcomm.2018.11.005).
- [30] Yadav, B. S.; Dasgupta, S. Effect of Time, PH, and Temperature on Kinetics for Adsorption of Methyl Orange Dye into the Modified Nitrate Intercalated MgAl LDH Adsorbent. *Inorg. Chem. Commun.* **2022**, *137*, 109203. DOI: [10.1016/j.inoche.2022.109203](https://doi.org/10.1016/j.inoche.2022.109203).
- [31] Shirkole, S. S.; Jayabalan, R.; Sutar, P. P. Dry Sterilization of Paprika (*Capsicum annuum* L.) by Short Time Intensive Microwave-Infrared Radiation: Part I - Establishment of Process Using Glass Transition, Sorption, and Quality Degradation Kinetic Parameters. *Innov. Food Sci. Emerg. Technol.* **2020**, *62*, 102345. DOI: [10.1016/j.ifset.2020.102345](https://doi.org/10.1016/j.ifset.2020.102345).
- [32] Finten, G.; Agüero, M. V.; Jagus, R. J.; Niranjan, K. High Hydrostatic Pressure Blanching of Baby Spinach (*Spinacia oleracea* L.). *LWT - Food Sci. Technol.* **2016**, *73*, 74–79. DOI: [10.1016/j.lwt.2016.05.043](https://doi.org/10.1016/j.lwt.2016.05.043).
- [33] Ramesh, M. N.; Wolf, W.; Tevini, D.; Bognár, A. Microwave Blanching of Vegetables. *J. Food Sci.* **2002**, *67*, 390–398. DOI: [10.1111/j.1365-2621.2002.tb11416.x](https://doi.org/10.1111/j.1365-2621.2002.tb11416.x).
- [34] Heaton, J. W.; Marangoni, A. G. Chlorophyll degradation in processed foods and senescent plant tissues. *Trends Food Sci. Technol.* **1996**, *7*, 8–15. DOI: [10.1016/0924-2244\(96\)81352-5](https://doi.org/10.1016/0924-2244(96)81352-5).
- [35] Hörtensteiner, S. Update on the Biochemistry of Chlorophyll Breakdown. *Plant Mol. Biol.* **2013**, *82*, 505–517. DOI: [10.1007/s11103-012-9940-z](https://doi.org/10.1007/s11103-012-9940-z).
- [36] Wang, J.; Xiao, H. W.; Fang, X. M.; Mujumdar, A. S.; Vidyarthi, S. K.; Xie, L. Effect of High-Humidity Hot Air Impingement Blanching and Pulsed Vacuum Drying on Phytochemicals Content, Antioxidant Capacity, Rehydration Kinetics and Ultrastructure of Thompson Seedless Grape. *Dry. Technol.* **2022**, *40*, 1013–1026. DOI: [10.1080/07373937.2020.1845721](https://doi.org/10.1080/07373937.2020.1845721).
- [37] Liu, Y.; Chen, W.; Fan, L. Effects of Different Drying Methods on the Storage Stability of Barley Grass Powder. *J. Sci. Food Agric.* **2022**, *102*, 1076–1084. DOI: [10.1002/jsfa.11443](https://doi.org/10.1002/jsfa.11443).
- [38] Vega-Gálvez, A.; Ah-Hen, K.; Chacana, M.; Vergara, J.; Martínez-Monzó, J.; García-Segovia, P.; Lemus-Mondaca, R.; Di Scala, K. Effect of Temperature and Air Velocity on Drying Kinetics, Antioxidant Capacity, Total Phenolic Content, Colour, Texture and Microstructure of Apple (Var. *Granny Smith*) Slices. *Food Chem.* **2012**, *132*, 51–59. DOI: [10.1016/j.foodchem.2011.10.029](https://doi.org/10.1016/j.foodchem.2011.10.029).
- [39] Lim, Y. Y.; Murtijaya, J. Antioxidant Properties of *Phyllanthus amarus* Extracts as Affected by Different Drying Methods. *LWT - Food Sci. Technol.* **2007**, *40*, 1664–1669. DOI: [10.1016/j.lwt.2006.12.013](https://doi.org/10.1016/j.lwt.2006.12.013).
- [40] Hamrouni-Sellami, I.; Rahali, F. Z.; Rebey, I. B.; Bourgou, S.; Limam, F.; Marzouk, B. Total Phenolics, Flavonoids, and Antioxidant Activity of Sage (*Salvia officinalis* L.) Plants as Affected by Different Drying Methods. *Food Bioprocess. Technol.* **2013**, *6*, 806–817. DOI: [10.1007/s11947-012-0877-7](https://doi.org/10.1007/s11947-012-0877-7).
- [41] Ismail, O.; Gökçe Kocabay, O. Vacuum Oven Drying of Mussels: Mathematical Modeling, Drying Characteristics and Kinetics Study. *Br. Food J.* **2021**, *124*, 1238–1253. DOI: [10.1108/BFJ-05-2021-0486](https://doi.org/10.1108/BFJ-05-2021-0486).
- [42] Kayran, S.; Brahim Doymaz, A. Infrared Drying of Apricot Pomace. *LAAR* **2019**, *49*, 213–218. DOI: [10.52292/j.laar.2019.199](https://doi.org/10.52292/j.laar.2019.199).
- [43] Derun, E. M. Infrared Drying Kinetics of Blue Mussels and Physical Properties. *Chem. Ind. Chem. Eng. Q.* **2019**, *25*, 1–10.
- [44] Inyang, U. E.; Oboh, I. O.; Etuk, B. R. Kinetic Models for Drying Techniques—Food Materials. *ACES* **2018**, *8*, 27–48. DOI: [10.4236/aces.2018.82003](https://doi.org/10.4236/aces.2018.82003).
- [45] Sadeghi, E.; Haghighi Asl, A.; Movagharnejad, K. Optimization and Quality Evaluation of Infrared-Dried Kiwifruit Slices. *Food Sci. Nutr.* **2020**, *8*, 720–734. DOI: [10.1002/fsn3.1253](https://doi.org/10.1002/fsn3.1253).
- [46] Doymaz, I.; Kipcak, A. S. Drying Characteristics Investigation of Black Mulberry Dried via Infrared Method. *J. Therm. Eng.* **2019**, *5*, 13–21. DOI: [10.18186/thermal.528969](https://doi.org/10.18186/thermal.528969).
- [47] Onwude, D. I.; Hashim, N.; Abdan, K.; Janius, R.; Chen, G. Modelling the Mid-Infrared Drying of Sweet Potato: Kinetics, Mass and Heat Transfer Parameters, and Energy Consumption. *Heat Mass Transfer* **2018**, *54*, 2917–2933. DOI: [10.1007/s00231-018-2338-y](https://doi.org/10.1007/s00231-018-2338-y).
- [48] Darvishi, H.; Farhudi, Z.; Behrooz-Khazaei, N. Multi-Objective Optimization of Savory Leaves Drying in Continuous Infrared-Hot Air Dryer by Response Surface Methodology and Desirability Function. *Comput. Electron. Agric.* **2020**, *168*, 105112. DOI: [10.1016/j.compag.2019.105112](https://doi.org/10.1016/j.compag.2019.105112).
- [49] Dincer, I.; Dost, S. An International Journal an Analytical Model for Moisture Diffusion in Solid Objects during Drying. *Dry. Technol.* **1995**, *13*, 425–435.

- [50] Rurush, E.; Alvarado, M.; Palacios, P.; Flores, Y.; Rojas, M. L.; Miano, A. C. Drying Kinetics of Blueberry Pulp and Mass Transfer Parameters: Effect of Hot Air and Refractance Window Drying at Different Temperatures. *J. Food Eng.* **2022**, 320, 110929. DOI: [10.1016/j.jfoodeng.2021.110929](https://doi.org/10.1016/j.jfoodeng.2021.110929).
- [51] Bezerra, C. V.; Meller Da Silva, L. H.; Corrêa, D. F.; Rodrigues, A. M. C. A Modeling Study for Moisture Diffusivities and Moisture Transfer Coefficients in Drying of Passion Fruit Peel. *Int. J. Heat Mass Transfer* **2015**, 85, 750–755. DOI: [10.1016/j.ijheat-masstransfer.2015.02.027](https://doi.org/10.1016/j.ijheat-masstransfer.2015.02.027).
- [52] Thummajitsakul, S.; Samaikam, S.; Tacha, S.; Silprasit, K. Study on FTIR Spectroscopy, Total Phenolic Content, Antioxidant Activity and Anti-Amylase Activity of Extracts and Different Tea Forms of *Garcinia schomburgkiana* Leaves. *LWT* **2020**, 134, 110005. DOI: [10.1016/j.lwt.2020.110005](https://doi.org/10.1016/j.lwt.2020.110005).
- [53] Kozłowicz, K.; Różyło, R.; Gładyszewska, B.; Matwijczuk, A.; Gładyszewski, G.; Chocyk, D.; Samborska, K.; Piekut, J.; Smolewska, M. Identification of Sugars and Phenolic Compounds in Honey Powders with the Use of GC–MS, FTIR Spectroscopy, and X-Ray Diffraction. *Sci. Rep.* **2020**, 10, 1–10. DOI: [10.1038/s41598-020-73306-7](https://doi.org/10.1038/s41598-020-73306-7).
- [54] Caunii, A.; Pribac, G.; Grozea, I.; Gaitin, D.; Samfira, I. Design of Optimal Solvent for Extraction of Bio-Active Ingredients from Six Varieties of *Medicago sativa*. *Chem. Cent. J.* **2012**, 6, 123–128. DOI: [10.1186/1752-153X-6-123](https://doi.org/10.1186/1752-153X-6-123).
- [55] Topala, C. M.; Tataru, L. D.; Ducu, C. ATR-FTIR Spectra Fingerprinting of Medicinal Herbs Extracts Prepared Using Microwave Extraction. *Arab. J. Med. Aromat. Plants* **2017**, 3, 1–9.
- [56] Yusuf, M.; Khan, R. A.; Khan, M.; Ahmed, B. Plausible Antioxidant Biomechanics and Anticonvulsant Pharmacological Activity of Brain-Targeted  $\beta$ -Carotene Nanoparticles. *Int. J. Nanomed.* **2012**, 7, 4311–4321. DOI: [10.2147/IJN.S34588](https://doi.org/10.2147/IJN.S34588).
- [57] Palma-Rodríguez, H. M.; Alvarez-Ramírez, J.; Vargas-Torres, A. Using Modified Starch/Maltodextrin Microparticles for Enhancing the Shelf Life of Ascorbic Acid by the Spray-Drying Method. *Starch/Staerke* **2018**, 70, 1700323. DOI: [10.1002/star.201700323](https://doi.org/10.1002/star.201700323).
- [58] Jendrzejewska, I. Application of X-Ray Powder Diffraction for Analysis of Selected Dietary Supplements Containing Magnesium and Calcium. *Front. Chem* **2020**, 8, 1–12. DOI: [10.3389/fchem.2020.00672](https://doi.org/10.3389/fchem.2020.00672).
- [59] Godswill, A. G.; Somtochukwu, I. V.; Ikechukwu, A. O.; Kate, E. C. Health Benefits of Micronutrients (Vitamins and Minerals) and Their Associated Deficiency Diseases: A Systematic Review. *IJF* **2020**, 3, 1–32. DOI: [10.47604/ijf.1024](https://doi.org/10.47604/ijf.1024).